Powder Technology 312 (2017) 321–333

Contents lists available at ScienceDirect

Powder Technology

journal homepage: www.elsevier.com/locate/powtec

The influence of surface roughness and adhesion on particle rolling

R. Wilson[a,*], D. Dini[b], B. Van Wachem[b]

[a] Department of Physics, The Blackett Laboratory, Imperial College London, South Kensington Campus, London SW7 2AZ, United Kingdom
[b] Department of Mechanical Engineering, City and Guilds Building, Imperial College London, South Kensington Campus, London SW7 2AZ, United Kingdom

ARTICLE INFO

Article history:
Received 15 September 2016
Received in revised form 25 January 2017
Accepted 28 January 2017
Available online 1 February 2017

Keywords:
Rolling resistance
Discrete element model
Surface roughness
Adhesion

ABSTRACT

The influence of surface roughness and contact adhesion on the rolling behaviour of dry particles has been investigated. Rough particle surfaces are approximated using an array of spheres, the properties of which are informed by random processes. An analytical model has been derived by considering the torques that a particle experiences. Two mechanisms of rolling resistance are explored – a stationary particle experiencing a tangential force, and a dynamically rolling particle. The analytical model is found to agree well with simulations of the equivalent system using the discrete element model. Adhesive forces are found to increase rolling resistance in all cases. The complex consequences of varying the height variance and length scale of the surface roughness are reproduced accurately by the analytical model.

© 2017 The Authors. Published by Elsevier B.V. This is an open access article under the CC BY license (http://creativecommons.org/licenses/by/4.0/).

1. Introduction

Many industrial and natural processes involve granular systems. Diverse phenomena such as avalanches [1], fluidized beds [2] and asthma inhalers [3] all depend on assemblies of small particles. However, due to the subtlety of interactions between the constituent grains, the behaviour of granular systems is complex and can be difficult to predict. Gaining a better knowledge of the mechanics of granular systems is therefore critical to the development of industrial processes, and the understanding of natural phenomena. Moreover, one would like to develop simple tools to study such systems, although some of the models required by these tools do not yet exist, or are not yet sufficiently accurate.

Real particles will always exhibit a degree of surface roughness. This has the effect of modifying the contact forces experienced during collisions [4], and can have a significant effect on the motion of a particle. Roughness is a phenomenon which typically occurs over many length scales [5]. Depending on the material, and on processes which have been applied to the surface, it is possible for a surface to exhibit roughness down to the atomic scale. Due to the wide range of forms that a rough surface may take, it is difficult to generalise the effect of roughness on a contact.

Of particular interest in this study is the behaviour of fine powders. The influence of adhesive forces on a particle can be found in the ratio of adhesive force ($\propto$ surface area) to weight ($\propto$ volume). A system of smaller grains will therefore experience more significant adhesive interactions. For dry powders with grains below $\sim$ 100μm Van der Waals interactions can no longer be treated as negligible [6]. In such cases the powder cannot flow as freely. This leads to behaviour such as bubbling in fluidized beds [2,6], and agglomeration [7].

It has relatively recently become possible to perform detailed simulations of granular flows. Frequently used methods include the Discrete Element Model [8] (DEM), or the treatment of particles as a continuous Eulerian phase [9]. In the present study, DEM is employed. It was chosen because it allows the physical properties of grains to be easily varied, and allows for relatively complex models to describe interactions on the scale of individual particles. The behaviour of a system is often strongly dependent on the interactions between grains, such that small changes on the particle scale can lead to large differences in system behaviour. It is therefore useful to know which properties are most influential, and to simulate them accurately.

In this work we focus on the resistance to rolling motion. Rolling resistance is critical to the behaviour of certain types of granular system. Sand piles, for example, can be strongly influenced by the magnitude of rolling resistance between particles. [10]. Additionally critical phenomena such as avalanches can be related to the presence of mechanisms which encourage collective, rather than individual, motion of particles – for instance friction and rolling resistance [11]. In particular, we study the influence of surface roughness and adhesive interactions on particle rolling.

1.1. Causes of rolling resistance

One factor that makes rolling resistance difficult to investigate is that a number of mechanisms may contribute to the observed

* Corresponding author.
E-mail address: robert.wilson12@imperial.ac.uk (R. Wilson).

http://dx.doi.org/10.1016/j.powtec.2017.01.080
0032-5910/© 2017 The Authors. Published by Elsevier B.V. This is an open access article under the CC BY license (http://creativecommons.org/licenses/by/4.0/).

phenomena. Any interaction which leads to an asymmetry in contact forces as a particle rolls may result in a torque which resists the rolling. The processes which most commonly lead to this situation are discussed presently.

Rolling resistance of a sphere may arise due to visco-elastic dissipation in the contact. This effect has been studied in detail, both analytically and using FEM simulations [12–15]. The visco-elastic force opposes the normal motion in the region of contact. As a sphere rolls on a plane, one half of the contact will be moving towards the plane, while the other half moves away. A torque is therefore induced by the opposing visco-elastic forces on either side of the contact. The same visco-elastic forces are responsible for energy dissipation during collisions, leading to a relationship between the collision dynamics and rolling behaviour of a sphere [15].

Contact plasticity may also play a part. In this instance the shape of either the particle, or the surface on which it rolls, is permanently deformed. Both cases lead to an extra 'bump' which the particle must surmount to continue rolling. This leads to an asymmetrical stress distribution when the particle rotates by a small amount, and therefore a torque. It has been observed that repeated rolls of a steel ball over the same surface of softer metal result in a decrease in rolling resistance. [16] This is consistent with the expected behaviour of rolling resistance due to plasticity, as the process of strain hardening reduces plastic deformation when the same area is repeatedly rolled over.

A third mechanism is adhesion, which can lead to energy dissipation while rolling. In the case of soft particles with large surface energies, there is a hysteresis effect as the particle comes in and out of contact. This is described by, for example, the Johnson-Kendall-Roberts (JKR) contact model [17]. The difference in force as the particle leaves contact leads to an energy dissipation associated with breaking adhesive bonds. The effect of this phenomenon on a rolling sphere has been taken into account [18,19], and found to result in a critical torque which must be applied before rolling occurs. When the adhesive energy is small compared to the energy required to cause significant elastic deformation there is no hysteresis; however, the additional normal force will modify the effects of viscoelastic and plastic interactions.

Finally, as a fourth mechanism, particle shape influences the rolling behaviour [20]. Stationary non-spherical particles may experience torques which resist applied tangential forces. Surface roughness does not introduce any dissipation, however can interact with other mechanisms to change the dissipation during rolling. For example, the moment induced by viscoelastic effects depend on the shape of the contact area.

In the present study we investigate the resistance to rolling due to the interplay between particle shape effects and adhesion. The focus is on rough, approximately spherical, grains. By characterising the roughness, we have developed analytical models to describe the torques experienced by a particle as it begins to roll, and in the case of a dynamically rolling particle. It is found that as well as shape and adhesion, viscoelasticity plays a significant role in some cases. These models are compared to numerical simulations of the equivalent rough particles, and the results discussed.

2. Theory

A number of models have been applied to spherical particles to describe the torque of rolling resistance, τ_r. Various assumptions on the mechanisms of energy dissipation and the source of torques lead to a number of analytical forms. The three most commonly used models are summarised below. Models tend to contain a coefficient of rolling resistance, μ_r, along with terms containing the particle radius, R, normal force, F_n, and angular velocity, $\boldsymbol{\omega}$.

A constant torque, opposing the rolling motion of the particle was proposed by Beer and Johnston [21]:

$$\boldsymbol{\tau}_r = -\mu_r R F_n \frac{\boldsymbol{\omega}}{|\boldsymbol{\omega}|}. \tag{1}$$

This form of rolling resistance has been used to study, amongst other things, the formation of sand piles [10,22]. While the behaviour of spheres is found to match well to experimental results, this model has the disadvantage that it leads to angular velocities which oscillate around $\boldsymbol{\omega} = 0$.

A second model treats rolling resistance as a damping effect. In this case the rolling resistance is proportional to the rate of rolling, as shown in Eq. (2), and leads to the exponential decay of $\boldsymbol{\omega}$. This analytic form can be found by investigating the viscous forces in a contact [12].

$$\boldsymbol{\tau}_r = -\mu_r R F_n \boldsymbol{\omega}. \tag{2}$$

An expression of this form is more stable than the constant torque model, as $\boldsymbol{\omega}$ is guaranteed to tend towards zero. However, according to the simulations of Zhou et al. [10] the behaviour of a sand pile using this model is not as realistic as that using the constant torque model of Eq. (1).

The third commonly used model takes a form similar to the Mindlin-Deresiewicz [23] model commonly used to model the frictional behaviour of spheres. A resistive torque initially increases linearly with the angle rolled, ϕ_r, with a constant of proportionality k_r. Upon reaching a threshold value, the torque is constant. These expressions are shown in Eq. (3).

$$\boldsymbol{\tau}_r = \begin{cases} -k_r \phi_r \frac{\boldsymbol{\omega}}{|\boldsymbol{\omega}|}, & \text{if } |\boldsymbol{\tau}_r| < \mu_r R F_n \\ -\mu_r R F_n \frac{\boldsymbol{\omega}}{|\boldsymbol{\omega}|}, & \text{otherwise.} \end{cases} \tag{3}$$

This model may also include a dissipative term of the form shown in Eq. (2). Without a dissipative term, this model tends to oscillate in a similar manner to the constant resistive torque shown in Eq. (1). These models have been compared in detail by Ai et al. [24].

A shortcoming of many existing models is that they rely on the coefficient of rolling resistance as a parameter, rather than prescribing a coefficient based on physical properties of the particles. It is frequently the case that the model is based on unrealistic assumptions – *e.g.* perfectly spherical particles – or must be fitted to experimental data. By considering particles with less idealised geometrical properties, the results of the current paper provide a better understanding of the influence of roughness and adhesion on rolling resistance.

2.1. Modelling of rough surfaces

A number of factors contribute to the geometry of a surface, including the chemical composition of the material, the method used to form the surface, and subsequent processes it may have been subject to. In order to model a generic rough surface, it is necessary to apply a number of constraints, as no mathematical model can describe every possible roughness. Several mathematical approaches have been developed [4,25-27] to describe rough surfaces.

Under light loading, contact between surfaces is made only at the peaks of the roughness profile. Models such as the Greenwood-Williamson [28] (GW) and Bush-Gibson-Thomas [25] model take advantage of this fact, approximating the asperities as spherical or ellipsoidal, and thereby greatly simplifying the contact problem. The Greenwood-Williamson model – a particular focus of the present study – treats asperities as spheres with a Gaussian distribution of heights. An alternative approach is to model the surface using random process theory [26]. In this case the statistical properties of a surface such as the average gradient and curvature may be derived analytically.

In the present study, surfaces are described using a model which is conceptually similar to the Greenwood-Williamson model. A rough surface is described using spherical asperities. Rather than consider the average loading behaviour of many asperities on a plane, we

consider the influence of relatively few asperities in contact on the surface of a sphere. The model contains a number of parameters which may be varied – the spacing and radius of spheres, as well as the mean and standard deviation of their heights – which do not correspond to easily measurable physical parameters. In order to constrain the parameter space to only those combinations which approximate realistic surfaces, it is useful to consider Nayak's analysis of correlated random fields [26]. It was shown by Nayak, and clarified by McCool [29], that the properties of peaks in a two-dimensional, isotropic, Gaussian, random field may be related to the parameters of the GW model.

Random fields are spaces in which the value at each point may be considered to be sampled from some probability distribution. The probability density of the height of the surface, z, at a given position, $\boldsymbol{r}$, is chosen to be a Gaussian distribution, denoted $\mathcal{N}$, with mean z_0 and standard deviation σ_z,

$$z \sim \mathcal{N}(z_0, \sigma_z^2). \tag{4}$$

Such a surface is also spatially correlated. Points on the surface will be distributed such that the expected value

$$E\left[z(\boldsymbol{r}_i)z(\boldsymbol{r}_j)\right] = R(\boldsymbol{r}_i, \boldsymbol{r}_j), \tag{5}$$

where $R(\boldsymbol{r}_i, \boldsymbol{r}_j)$ is the auto-correlation function. For an isotropic random surface, the correlation is a function of only the distance $r = |\boldsymbol{r}_j - \boldsymbol{r}_i|$, and thus does not depend on the absolute positions of the two points. Applying a Fourier transform to the auto-correlation function yields the power spectral density, which exhibits a number of useful characteristics. Specifically, the zeroth, second and fourth moments of the power spectral density, m_0, m_2 and m_4, correspond to measurable properties of a surface. m_0 corresponds to the profile variance, σ_z^2, while m_2 and m_4 are the mean square gradient and curvature experienced along a straight line traced in an arbitrary direction on the surface [29]. The choice of auto-correlation function determines the structure of the roughness. Common choices of auto-correlation function include an exponential decay and a Gaussian distribution.

In this case a Gaussian auto-correlation function is chosen, as it allows moments to be calculated analytically. Consider a 2D random field, in which heights are distributed according to a Gaussian distribution with a mean, z_0, and standard deviation, σ_z. The auto-correlation function is a Gaussian with a mean of 0, and a standard deviation, l_c, which will be referred to as the correlation length. The power spectral density then has the form

$$\Phi(k) = \frac{\sigma_z^2 l_c}{2\pi} \exp\left(\frac{-l_c^2 k^2}{2}\right). \tag{6}$$

This is an expression of the relative prominence of undulations as a function of their wavelength, λ, parametrised by the wavenumber $k = \frac{2\pi}{\lambda}$. The moments of Eq. (6) can be evaluated to yield the following relationships:

$$\begin{aligned} m_0 &= \sigma_z^2 \\ m_2 &= \frac{\sigma_z^2}{l_c^2} \\ m_4 &= 3\frac{\sigma_z^2}{l_c^4} \end{aligned} \tag{7}$$

The moments in Eq. (7) can in turn be related to the properties of the GW model [25,26,29]. We assume that asperities in the GW model correspond to the highest points of a real rough surface. The statistics of peaks on a random field are therefore used to inform the size and placement of the asperities in the GW model. The density of peaks, D_p, mean peak height, $\bar{z}_\mathrm{p}$, mean peak curvature, $\bar{\kappa}_\mathrm{p}$, and variance of peak heights, σ_p^2, are given by McCool as [29]:

$$D_\mathrm{p} = \frac{m_4}{6\pi\sqrt{3}m_2} = \frac{\sqrt{3}}{6\pi l_c^2}, \tag{8}$$

$$\bar{z}_\mathrm{p} = z_0 + \frac{4m_2}{\sqrt{\pi m_4}} = z_0 + \frac{4\sigma_z}{\sqrt{3\pi}}, \tag{9}$$

$$\bar{\kappa}_\mathrm{p} = \frac{8}{3}\sqrt{\frac{m_4}{\pi}} = \frac{8\sigma_z}{\sqrt{3\pi}l_c^2}, \tag{10}$$

$$\sigma_\mathrm{p}^2 = m_0 - \frac{0.8969 m_2^2}{m_4} = 0.7011\sigma_z^2. \tag{11}$$

These expressions can be used to inform the choice of parameters in the GW model. D_p, $\bar{z}_\mathrm{p}$, and σ_p can be used directly to describe the density, average height, and height variation of asperities, while taking the reciprocal of $\bar{\kappa}_\mathrm{p}$ gives a value for the mean peak radius, $\bar{r}_\mathrm{p}$ – and thus the asperity radius in the GW model.

In order to model a rough sphere, rather than the rough plane described by the GW model, a number of changes must be made. The average height, z_0, is replaced by the average radius, R_0. Similarly, the standard deviation in height σ_z is replaced by the standard deviation of radius, σ_r.

3. Computational framework

Simulations of particulate systems may be performed using the discrete element model. In this scheme each particle is treated as a Newtonian element – frequently a sphere – and its motion integrated numerically. The current study employs a 'soft-sphere' type collision model [30]. In this model, when two particles overlap one another a force is applied which depends on the magnitude of the overlap.

In the case of spheres each particle can by characterised by its mass, m, position, $\boldsymbol{r}$, moment of inertia, $\boldsymbol{I}$, and angular velocity, $\boldsymbol{\omega}$. Particles experiences a body force due to gravity, $m\boldsymbol{g}$, contact forces where it overlaps other particles or walls, $\boldsymbol{f}_c$, and torques due to tangential forces at the contacts, $\boldsymbol{\tau}_c$. The translation and rotation of each particle are governed by the equations

$$m\ddot{\boldsymbol{r}} = m\boldsymbol{g} + \boldsymbol{f}_c, \tag{12}$$

$$I\dot{\boldsymbol{\omega}} = \boldsymbol{\tau}_c. \tag{13}$$

These are integrated using a Verlet scheme. The contact force, $\boldsymbol{f}_c$, may be decomposed into a normal and tangential component, $\boldsymbol{f}_n$ and $\boldsymbol{f}_t$ respectively, which will be discussed presently.

3.1. Normal forces

There are a number of approaches which may be used to describe soft-sphere particle-particle interactions in DEM. The original model, proposed by Cundall and Strack [8], prescribed a damped spring normal contact force. In the present study a nonlinear force based on the Hertzian contact model [31] is used. A number of contact models based on Hertz' solution have been developed, differing in their approaches and approximations [30,32-35]. While nonlinear contact models tend to use the Hertzian normal force, their treatment of tangential and dissipative forces often vary.

In principal any force model may be used in DEM, in this instance we have selected the commonly used non-linear normal force model proposed by Tsuji et al. [30]. The normal force in this model, $\boldsymbol{f}_n$, is

expressed in terms of the overlap, δ, the normal component of the velocity, $\boldsymbol{v}_n$, and the adhesive force, $\boldsymbol{f}_{\text{adh}}$.

$$\boldsymbol{f}_n = K_n\delta_n^{3/2}\hat{\boldsymbol{n}} - \eta_n\boldsymbol{v}_n + \boldsymbol{f}_{adh}, \tag{14}$$

where K_n and η_n are the stiffness and damping coefficients respectively, and take the physical properties of the particles into account, and $\hat{\boldsymbol{n}}$ is the unit vector from the centre of the collision to the particle centre. For a collision between two particles, denoted by subscripts 1 and 2, the reduced radius, $R^* = \frac{R_1R_2}{R_1+R_2}$, and reduced elastic modulus $E^* = \frac{E_1E_2}{E_1(1-\nu_2^2)+E_2(1-\nu_1^2)}$ are used. η_n also depends on the particle mass, m. The stiffness and damping coefficients can be expressed as:

$$K_n = \frac{4}{3}E^*\sqrt{R^*}, \tag{15}$$

$$\eta_n = \alpha(mK_n)^{1/2}\delta_n^{1/4}. \tag{16}$$

α allows the dissipation to be modified independent of the other parameters, and takes a value of $0 < \alpha < 1$.

Adhesive forces between particles are taken into account via the work of adhesion, $\Delta\gamma$. If two surfaces have a surface energies of γ_1 and γ_2 associated with them when alone in a vacuum, and the two surfaces when in contact have an energy of γ_{12}, $\Delta\gamma$ is defined as

$$\Delta\gamma = \gamma_1 + \gamma_2 - \gamma_{12}. \tag{17}$$

This parameter measures how energetically favourable it is for two surfaces to stick together, and therefore the strength of adhesion between them.

In DEM, adhesion between spheres is frequently taken into account by using the model proposed by Johnson, Kendall and Roberts [17] (the JKR model), or that of Derjaguin, Muller and Toporov [36,37] (the DMT model). Alternatively, as adhesive interactions between fine powders usually occur due to the Van der Waals force, it is common to consider a truncated version of Hamaker's equation [38]. Whether a system is described best by the JKR or DMT model was established by Tabor [39] to depend on the parameter $\mu = \left(\frac{R^*\Delta\gamma^2}{E^{*2}\varepsilon^3}\right)^{1/3}$. In this expression ε is the equilibrium spacing between the atoms which make up the surfaces. A particle with $\mu \gg 1$ will be best described by the JKR model, and $\mu \ll 1$ by DMT. In this case small particles with relatively small adhesive energies are considered, and the DMT model is therefore to be preferred.

The adhesive force prescribed by the DMT model increases in magnitude as the overlap between two particles increases. [37] For values of $\mu > 0.24$ this leads to an increase in pull-off force, which is the opposite trend to that which is obtained by numerical simulation. [40] It can therefore be concluded that Maugis' far simpler approach to the DMT model [41] – a constant adhesive force of $2\pi R^*\Delta\gamma$– is not less accurate than the original formulation. Adhesive forces are presently modelled in this manner. This leads to the following expressions for f_{adh}, and contact radius, a, under an external load on the contact of P:

$$f_{\text{adh}} = -2\pi R^*\Delta\gamma\hat{\boldsymbol{n}}. \tag{18}$$

$$\frac{3E^*a^3}{4R^*} = P + 2\pi R^*\Delta\gamma \tag{19}$$

3.2. Tangential forces

When a particle in contact undergoes motion in a direction perpendicular to the contact normal, it will experience a frictional force. The magnitude of this force is related to the area of the contact [17,42]. Frictional forces between spheres are usually treated using the Mindlin-Deresiewicz model [23].

Tangential forces, $\boldsymbol{f}_t$, are described using a linear spring and dashpot, with a coulomb type mechanism for sliding [23]. Relevant parameters are the tangential spring constant, k_t, tangential displacement, $\boldsymbol{\delta}_t$, slip velocity, $\boldsymbol{v}_s$, and coefficient of friction, μ_f. Under an external load of P, the tangential force is:

$$\boldsymbol{f}_t = \begin{cases} -k_t\boldsymbol{\delta}_t - \eta_t\boldsymbol{v}_s & \text{if } |\boldsymbol{f}_t| < \mu_f|\boldsymbol{f}_n|, \\ -\mu_f(P + 2\pi R^*\Delta\gamma)\hat{\boldsymbol{t}} & \text{otherwise,} \end{cases} \tag{20}$$

where $\hat{\boldsymbol{t}}$ opposes the direction of sliding. The tangential drag coefficient, η_t, is calculated from material properties in a similar way to η_n:

$$\eta_t = \alpha\sqrt{mK_t}\delta_t^{1/4}, \text{ where} \tag{21}$$

$$K_t = 8\sqrt{R^*\delta_n}G^*. \tag{22}$$

G^* is the equivalent of E^* for the shear modulus, G.

In the presence of adhesive interactions, the slip behaviour within the contact can become much more complex, as there are areas of positive and negative pressure. While in the case of JKR type particles the particle deformation at the contact is significantly different from the Hertzian solution, in the low Tabor parameter regime this is not the case. As the contact stays close to the Hertzian shape [43], it is a good approximation to use the standard Mindlin-Deresiewicz based friction model.

3.3. Rough particle modelling using compound particles

It is not straightforward to represent a detailed rough surface for a particle in a DEM simulation. However, the simulation of 'compound particles' within the DEM framework [44,45] has been an active area of research in recent years. By overlapping a number of spheres, and imposing that they move as a unit, it is possible to simulate non-spherical geometries. This approach is popular for simulating systems such as ellipses and rods, as well as other geometries [44], which better represent physical particles. It is also well suited to simulating nearly spherical particles with a Greenwood-Williamson type roughness. In this case, asperities are modelled by small spheres, attached to the surface of a larger central sphere.

The moment of inertia, I, is a second order tensor. Due to the symmetry of spheres their moment of inertia can be reduced to a scalar and calculated analytically. For general geometries this is not the case, and it is therefore necessary to calculate I numerically by integrating over the volume of the body.

For a sphere all orientations are indistinguishable, and it is therefore sufficient to consider only the angular velocity, without the absolute rotation. However, for a non-spherical particle such as a compound arrangement of spheres, the orientation must also be tracked. There are a number of methods for mathematically describing orientations and rotations in 3D space. In the present study a Quaternion based method, as described by Zhao and Van Wachem [46], is employed.

3.4. Generation of rough particles

Rough particles are generated to match the desired Gaussian surface as closely as possible. This surface may be statistically defined by its average radius, R_0, standard deviation of surface height, σ_r, and correlation length, l_c. Alternatively, the moments of the surface profile, m_0, m_2 and m_4, may be used.

The rough particle is generated by evenly distributing smaller spheres of radius r_{p} on a larger sphere, see for example Fig. 1. It

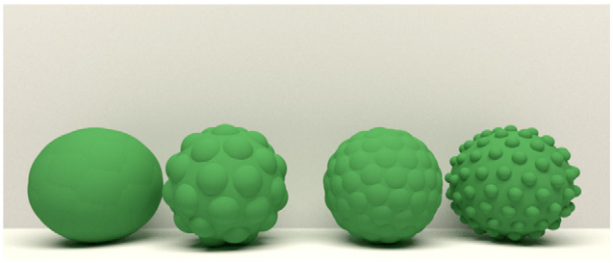


Fig. 1. Simulated rough particles. The particle surfaces have a correlation length, l_c, and surface height standard deviation, σ_r, of (from left to right) $\sigma_r = 0.5$ μm, $l_c = 6.5$μm; $\sigma_r = 1.5$ μm, $l_c = 6.5$μm; $\sigma_r = 0.5$ μm, $l_c = 4.5$μm; $\sigma_r = 1.5$ μm, $l_c = 4.5$μm.

has been found that if the large central sphere is given a radius of R_0, for certain values of σ_r and l_c it will come into contact with the plane upon which the particle sits. This is not ideal, as contact is only desired at the asperities. A better radius for the large central sphere is the average radius of the troughs of the rough surface. In a manner similar to the average peak height given by Eq. (9), this can be expressed as $R_c = R_0 - \frac{4\sigma_r}{\sqrt{3\pi}}$.

The number of asperities to be placed on a particle can be derived from the density of peaks, Eq. (8). Each asperity will have an area of $A_{asp} = 1/D_p$ associated with it. When distributed over the surface of a sphere of radius R_0, the number of asperities will be

$$\frac{2R_0^2}{\sqrt{3}l_c^2} \tag{23}$$

In practice this expression must be rounded to the nearest integer.

Each asperity has a radius, r_p, given by the reciprocal of the mean peak curvature expressed in Eq. (10). The radius at which the asperities are placed, R_{asp}, is given by subtracting this radius from the mean peak height. These parameters can therefore be expressed as

$$r_p = \frac{1}{\bar{\kappa}_p} = \frac{\sqrt{3\pi}l_c^2}{8\sigma_r}, \tag{24}$$

$$R_{asp} = \bar{z}_p - r_{asp} = R_0 + \frac{4\sigma_r}{\sqrt{3\pi}} - \frac{\sqrt{3\pi}l_c^2}{8\sigma_r}. \tag{25}$$

A key feature of the original GW model is that asperity heights followed a Gaussian distribution, with a standard deviation given by Eq. (11). In the present study, we consider all asperities to sit at the same radius of r_{asp}. As a result of this, the analytic model described in Section 4 is simplified, and the numerical simulations in Section 5 are more consistent. As we are aiming to describe the average behaviour of such particles, the exclusion of height variation is not thought to make a significant difference.

To distribute a number of points evenly across a sphere is not trivial. For specific numbers of points the optimal solution is to construct a geodesic sphere – a distribution whereby each point has an approximately equal area associated with it. Geodesic spheres allow numbers of points, N, of $N = 10n^2 + 2$, for positive integers, n. This imposes a significant constraint of the number of points which can be placed, and is therefore not an appropriate solution if an arbitrary range of surface properties is required.

The solution implemented presently involves treating points as Newtonian particles which experience both a long ranged, repulsive, pair-wise potential, and a damping force proportional to their velocity. They are constrained to the surface of a sphere. These particles are first placed on the sphere using the Marsaglia method [47]. The system is then allowed to relax such that the total energy reaches a minimum value, which leads to an arrangement of points that is approximately uniform. In this case, two particles experience an electrostatic type potential, and are treated in a Newtonian fashion as time is integrated. When the change in energy per timestep falls below a threshold value, the particles are assumed to be in an optimal configuration and the asperities are placed on their positions – scaled to the correct radius. Examples of particles generated in this manner are shown in Fig. 1.

Due to limitations in the compound particle method, it is difficult to simulate particles in greater detail than the most coarse scale of roughness. To simulate a rough particle more accurately, it would be necessary to use spheres of increasingly small radii to reproduce the multi-scale nature of a rough surface. However, it is thought that the largest roughness scale will contribute most significantly to the rolling resistance of a particle.

4. Analytical model

A rough particle at rest will have multiple contacts with a flat plane. It is therefore likely that an uneven distribution of forces across these contacts will lead to torques which resist rolling motion. Because of this, a form of behaviour similar to the third type of rolling resistance discussed in Section 2 is expected. A value for the critical torque, and the angle at which this torque occurs are derived in Section 4.1 by considering the system geometry and forces.

Additionally, as a rough particle rolls, unbalanced dissipative forces in the contacts will lead to a resistive torque, which counteracts the motion. This phenomena is discussed in more detail, and described mathematically, in Section 4.2.

4.1. Resistance to rolling on a stationary particle

To calculate the minimum force required to roll a rough particle, it is useful to first consider the case of a 2 dimensional system. A 2D rough particle is modelled as a number of overlapping disks; one in the centre, and one for each asperity on the surface, as shown in Fig. 2. This particle sits on a flat surface, and experiences forces acting at the centre of mass, and at the contact points.

The normal and tangential body forces, $\boldsymbol{F}_n$ and $\boldsymbol{F}_t$, are defined as the components of the force acting at the centre of mass of the particle in the directions perpendicular and parallel to the plane respectively. These forces may occur due to, for example, the action of gravity on a particle on an inclined plane. Additionally each asperity in contact with the plane, denoted i, experiences a contact force, $\boldsymbol{f}_c^i$. Each $\boldsymbol{f}_c^i$ can also be decomposed into the normal force, $\boldsymbol{f}_n^i$, due to elastic and adhesive interactions, and the frictional tangential force, $\boldsymbol{f}_t^i$. In a state of equilibrium, it is necessary that these forces balance:

$$\boldsymbol{F}_n + \sum_i \boldsymbol{f}_n^i = 0, \tag{26}$$

$$\boldsymbol{F}_t + \sum_i \boldsymbol{f}_t^i = 0. \tag{27}$$

$\boldsymbol{F}_n$ and $\boldsymbol{F}_t$ act at the centre of mass, and therefore do not cause a torque. The contact forces, on the other hand, may lead to torques. It is useful to decompose these into the torque due to normal forces, and those due to the tangential components. The vector from the centre of mass to each contact point, $\boldsymbol{d}^i$, can be decomposed into a distance normal and tangential to the plane, $\boldsymbol{d}_n^i$ and $\boldsymbol{d}_t^i$.

Tangential contact forces apply a torque of

$$\boldsymbol{\tau}_t = \sum_i \boldsymbol{d}_n^i \times \boldsymbol{f}_t^i, \tag{28}$$

while the torque due to normal contact forces is given by

$$\boldsymbol{\tau}_n = \sum_i \boldsymbol{d}_t^i \times \boldsymbol{f}_n^i. \tag{29}$$

It should be noted that $\boldsymbol{\tau}_t$ is entirely due to the frictional response to the tangential body force, $\boldsymbol{F}_t$, while $\boldsymbol{\tau}_n$ arises from asymmetry in the distribution of normal contact forces. In equilibrium, these torques sum to zero.

It is assumed that the particle in its equilibrium resting position will make contact at exactly 2 points, positioned equal distances either side of the centre of mass. While this may not be the case for large normal forces or roughnesses with short length scales, the following analysis is constrained to cases in which this is a valid approximation. Such a particle will be able to resist tangential forces up to a point – an applied $\boldsymbol{F}_t$ will induce a small rotation, leading to asymmetry in the contact forces and resulting in a resistive torque. For very small rotations both asperities will still be in contact, but one will experience a greater elastic deformation, and therefore higher contact force. This contact is said to be 'leading', while the other is 'trailing'. At some point the trailing asperity will come out of contact completely. Further rotation will then only decrease the distance, $|\boldsymbol{d}_t|$, to the leading asperity, resulting in a reduction to the resistive torque. The maximum torque a particle can resist before rolling, $\boldsymbol{\tau}^{\text{crit}}$, will therefore occur just as the trailing asperity comes out of contact.

The magnitude of $\boldsymbol{\tau}^{\text{crit}}$ may be calculated by considering the forces which occur when the particle is in equilibrium. It will correspond to a maximum applied tangential force, $\boldsymbol{F}_t^{\text{crit}}$, taking a value of $\boldsymbol{\tau}^{\text{crit}} = \boldsymbol{d}_n \times \boldsymbol{F}_t^{\text{crit}}$. We assume that the trailing asperity is just touching the plain. It is still close enough to experience adhesive forces, but does not support any normal or tangential contact forces, as shown in Fig. 2. With the leading contact denoted by the superscript 1, and the trailing contact by 2, Eqs. (26) and 27 can be used to find values for $\boldsymbol{f}_n^1$ and $\boldsymbol{f}_t^1$.

$$\boldsymbol{f}_n^1 = -\left(\boldsymbol{F}_n + \boldsymbol{f}_{\text{adh}}^2\right), \text{ and} \tag{30}$$

$$\boldsymbol{f}_t^1 = -\boldsymbol{F}_t^{\text{crit}}. \tag{31}$$

Torques arising from these two forces will sum to zero:

$$-\boldsymbol{d}_n \times \boldsymbol{F}_t^{\text{crit}} - \boldsymbol{d}_t^1 \times (\boldsymbol{F}_n + \boldsymbol{f}_{\text{adh}}^2) + \boldsymbol{d}_t^2 \times \boldsymbol{f}_{\text{adh}}^2 = 0. \tag{32}$$

As the system is symmetric, it can be seen that $\boldsymbol{d}_t^1 = -\boldsymbol{d}_t^2 := \boldsymbol{d}_t$. Eq. (32) is thereby simplified to

$$\boldsymbol{d}_n \times \boldsymbol{F}_t^{\text{crit}} + \boldsymbol{d}_t \times (\boldsymbol{F}_n + 2\boldsymbol{f}_{\text{adh}}^2) = 0. \tag{33}$$

From this it follows that

$$|\boldsymbol{\tau}^{\text{crit}}| = |\boldsymbol{d}_t||\boldsymbol{F}_n + 2\boldsymbol{f}_{\text{adh}}^2|. \tag{34}$$

The critical angle at which $\boldsymbol{\tau}^{\text{crit}}$ occurs, ϕ^{crit}, can be approximated analytically in a similar manner to the force. For a 2D system we have already seen that the maximum resistive torque occurs at the point when the trailing asperity has just come out of contact. The angle will depend on the overlap between the lead asperity and the plane, which is a function of the total load, P, experienced by the contact, where

$$\boldsymbol{P} = \boldsymbol{F}_n + \boldsymbol{f}_{adh}^2 \tag{35}$$

In the present analysis a Hertzian contact model is considered, with an additional adhesive component, however the same principle can be applied to other models.

For a leading contact overlapping by a distance δ_n, with a total distance between the contacts of $2|\boldsymbol{d}_t|$, there is an angle of

$$\tan(\phi^{\text{crit}}) = \frac{\delta_n}{2|\boldsymbol{d}_t|} \approx \phi^{\text{crit}}. \tag{36}$$

In almost all cases δ_n will be sufficiently small compared to $|\boldsymbol{d}_t|$ to warrant the small angle approximation on ϕ^{crit}. As the deformation is assumed to be Hertzian the overlap is given by $\delta_n = a^2/R^*$,

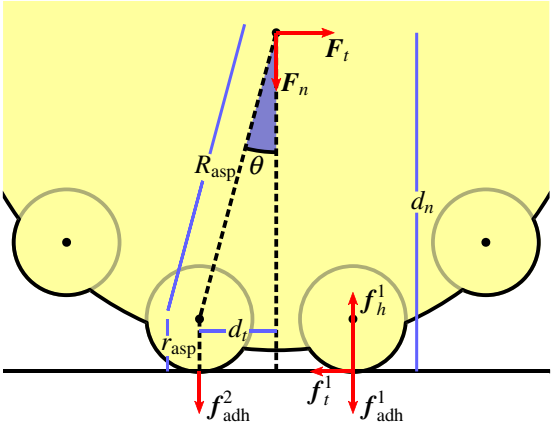


Fig. 2. The forces acting on a static particle under a tangential load at the critical point where the rear asperity is only just in contact. The body forces F_n and F_t act at the centre of mass. These are balanced by the contact forces due to elastic deformation, f_h, adhesive interactions, f_{adh}, and friction, f_t, at the contacts. The contacts are labelled by superscripts 1 and 2. Also labelled are the geometrical properties required to calculate the torque applied by these contact forces.

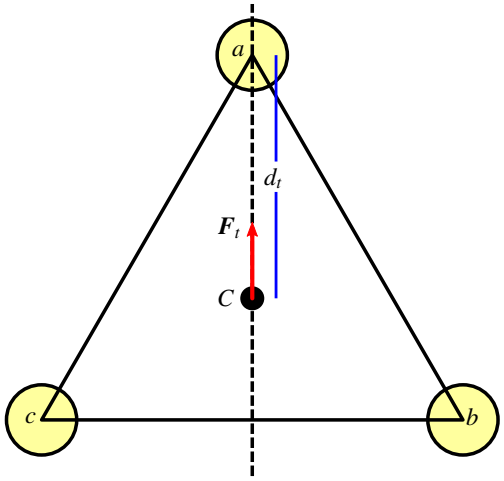


Fig. 3. The contact points of a 3D rough particle. Yellow circles are areas of contact, and the centre of mass is directly above the centre of the triangle, C. F_t acts parallel to a symmetry plane, and may point directly towards or away from any of the three asperities in contact, a, b and c.

where a is the contact radius, introduced in Eq. (19). Combining these expressions gives:

$$\delta_n = \left(\frac{3|\boldsymbol{P} + \boldsymbol{f}^1_{adh}|}{4E^* \sqrt{R^*}} \right)^{\frac{2}{3}}. \tag{37}$$

It is necessary to know the value of the adhesive force at both contacts. As discussed in Section 3.1, we approximate that the adhesive force is independent of contact deformation, thus $\boldsymbol{f}^1_{\text{adh}} = \boldsymbol{f}^2_{\text{adh}} := \boldsymbol{f}_{\text{adh}}$.

The distances $\boldsymbol{d}_t$ and $\boldsymbol{d}_n$ can be expressed in terms of the geometry of the particle. The relevant parameters are the radius of the asperity disks, r_{asp}, the radius at which the asperity disks are positioned, R_{asp}, and the angle, θ, from the centre of the contact to the centre of the sphere representing an asperity. These are illustrated in Fig. 2. For a particle resting on two asperities, the distance from the centre to the plane upon which it rests is given by

$$|\boldsymbol{d}_n| = R_{\text{asp}} \cos(\theta) + r_{\text{asp}}, \tag{38}$$

while the distance parallel to the plane from the centre to one of the asperities in contact is

$$|\boldsymbol{d}_t| = R_{\text{asp}} \sin(\theta). \tag{39}$$

4.1.1. Generalisation to 3D rough particles

The model presented for the resistance to rotation in 2D rough particles can be adapted to describe 3D particles, although a number of approximations are necessary to simplify the derivation. In the 2D case it is assumed that a particle in equilibrium would make contact with a plane at two points. Similarly, for a 3D particle we assume that three asperities make contact. It is further assumed that asperities are distributed evenly on the surface, *i.e.* that the minimum distance between neighbouring asperities is maximised. If this is the case, the contact points will sit approximately on the vertices of an equilateral triangle, as shown in Fig. 3.

$\boldsymbol{F}_t$ can be applied in any direction parallel to the plane. Even with the assumption of an equilateral triangle of contact points, the critical torque which can resist a tangential force in an arbitrary direction is difficult to determine. The simplest case is when $\boldsymbol{F}_t$ is applied parallel to one of the triangle's plains of symmetry. In this case an expression similar to Eq. (34) can be derived. The direction of $\boldsymbol{F}_t$ shown in Fig. 3 is that which leads to the highest magnitude of $\boldsymbol{\tau}^{max}$, while the smallest $\boldsymbol{\tau}^{max}$ is found when $\boldsymbol{F}_t$ is applied in the opposite direction.

The vectors from C to each of the contacts, $\boldsymbol{d}^i_t$, have the same magnitude, d_t. Meanwhile, the vector from C to the centre of the line joining two contacts has a magnitude of $\frac{d_t}{2}$. If the centre of mass of the rough particle is labelled O, and the centre of the sphere representing one of the asperities in contact is A, the distances d_t and d_n can be expressed in terms of the angle $\theta_{3D} = \angle AOC$, where C is labelled in Fig. 3. In this case the 2D Eqs. (38) and 39 may be used, with θ_{3D} replacing θ.

θ_{3D} is calculated by considering the arrangement of asperities on the surface. For simplicity we assume that the geometry of asperities on a sphere can be approximated by that of asperities on a plane. In this case, if asperities form a hexagonal lattice and each has an area of A_{asp} associated with it, the distance d_t can be approximated as

$$d_t = \sqrt{\frac{4\pi l_c^2}{3}}. \tag{40}$$

Assuming that θ_{3D} is sufficiently small, it can be approximated as

$$\theta_{3D} \approx \frac{d_t}{R_0} = \sqrt{\frac{4\pi}{3}} \frac{l_c}{R_0}. \tag{41}$$

For the case shown in Fig. 3, we consider the situation where asperities b and c are only just in contact. Then at each contact there is an adhesive force of f_{adh}, and contact a experiences a total normal load of

$$\boldsymbol{P} = \boldsymbol{F}_n + 2\boldsymbol{f}_{\text{adh}}. \tag{42}$$

If $\boldsymbol{F}_t$ is balanced by the frictional force at a, the maximum magnitude of the torque from the contacts is

$$\begin{aligned} \boldsymbol{\tau}^{\text{crit}} &= d_t |\boldsymbol{P}| + \frac{d_t}{2} 2 |\boldsymbol{f}_{\text{adh}}| \\ &= d_t \left(|\boldsymbol{F}_n + 3|\boldsymbol{f}_{\text{adh}}| \right). \end{aligned} \tag{43}$$

Similarly, if $\boldsymbol{F}_t$ is applied in the opposite direction contacts b and c are leading, while a trails. The magnitude of the maximum torque that can be resisted is

$$\boldsymbol{\tau}^{\text{crit}} = \frac{d_t}{2} \left(|\boldsymbol{F}_n + 3\boldsymbol{f}_{\text{adh}}| \right). \tag{44}$$

These represent the extreme values of the critical torque, *i.e.* the directions in which it is easiest and most difficult to roll the particle. The mean value of $\boldsymbol{\tau}^{\text{crit}}$, averaged over possible orientations of tangential force, would fall somewhere between Eqs. (43) and (44). It is therefore expressed as

$$\bar{\boldsymbol{\tau}}^{\text{crit}} = \lambda_{\boldsymbol{\tau}} d_t \left(|\boldsymbol{F}_n + 3\boldsymbol{f}_{\text{adh}}| \right), \tag{45}$$

where $\lambda_{\boldsymbol{\tau}}$ is a constant in the range $0.5 < \lambda_{\boldsymbol{\tau}} < 1$.

For the critical angle in the 3D case a similar approach is taken. The distance from one vertex of the triangle of contact points to the midpoint of the other two vertices is $\frac{3d_t}{2}$. The total load experienced at this contact is that of Eq. (42). If the particle is rolled in the opposite direction, this force will be shared equally between two contacts.

In the case of $\boldsymbol{F}_t$ applied towards a contact point,

$$\phi^{\text{crit}} = \frac{2\left(\frac{3|\boldsymbol{P} + \boldsymbol{f}_{adh}|}{4E^* \sqrt{R^*}} \right)^{\frac{2}{3}}}{3d_t}. \tag{46}$$

If $\boldsymbol{F}_t$ is in the opposite direction, each leading asperity experiences a normal force of $|f_n|/2$, and the value of ϕ^{crit} is therefore reduced by a factor of $\frac{1}{2}^{2/3}$. As these represent the extreme values, the average angle, $\bar{\phi}^{\text{crit}}$, over all orientations of $\boldsymbol{F}_t$, will fall between them, and can be expressed as

$$\bar{\phi}^{\text{crit}} = \lambda_\phi \frac{2\left(\frac{3|\boldsymbol{P} + \boldsymbol{f}_{adh}|}{4E^* \sqrt{R^*}} \right)^{\frac{2}{3}}}{3d_t}. \tag{47}$$

where $0.63 < \lambda_\phi < 1$.

4.2. Deceleration of rolling rough particles

As a rough particle rolls in the absence of an external force, it decelerates. To find the mechanism for this deceleration, it is necessary to consider the unbalanced torques which a particle experiences as it rolls. We consider the case in which continuous contact exists at

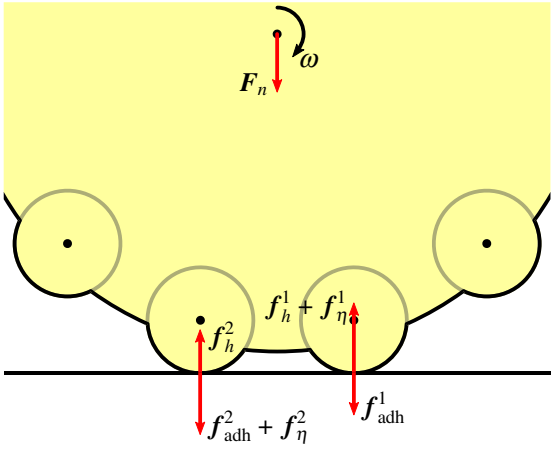


Fig. 4. The normal forces acting on a particle rolling with angular speed $\boldsymbol{\omega}$. Asymmetry caused by the opposing signs of the viscous force lead to a torque which opposes the direction of rolling.

all times, *i.e.* the particle is not bouncing. Once again, a two dimensional system is first considered to reduce the complexity of the problem.

The tangential forces due to friction at contact points between the asperities of the moving particle and the plane generate the torque which causes the particle to roll. Normal elastic forces acting at the contact points contribute either an accelerating or decelerating torque depending on the orientation of the particle. It is expected that over the course of an entire revolution these torques average to zero. The only torque which is unbalanced, and causes the particle to decelerate, is the velocity dependent viscous force, $\boldsymbol{f}_\eta$, in the contact model. This torque is negligible in the previously considered case of a stationary particle, as the velocity of the particle is assumed to be zero in that case.

The decelerating torque averaged over one revolution, $\bar{\boldsymbol{\tau}}_{\text{decel}}$ of the particle as it rolls can therefore be expressed as the average decelerating viscous torque per asperity, $\bar{\boldsymbol{\tau}}_{\text{asp}}$, multiplied by the number of asperities per revolution, $n_{2\pi}$:

$$\bar{\boldsymbol{\tau}}_{\text{decel}} = n_{2\pi}\bar{\boldsymbol{\tau}}_{\text{asp}}. \tag{48}$$

To calculate the average decelerating torque per asperity analytically is a difficult problem, as there is a constantly changing normal velocity at each contact, and at times more than one simultaneous contact. Due to the difficulties in evaluating this torque exactly, even in the relatively simple 2D system, it is necessary to approximate it. The point at which one asperity has just come into contact, and a second is about to leave contact is considered. This situation is illustrated in Fig. 4. It is thought that this is the point where the torque exerted is a maximum, as when only one asperity is in contact the velocity in the normal direction is very small, and therefore will not lead to a large viscoelastic force. $\bar{\boldsymbol{\tau}}_{\text{asp}}$ can then be approximated as some fraction of this maximum torque.

A symmetrical situation in which a particle sits on two asperities, both overlapping the plane by an amount δ_n, and rotates with angular velocity $\boldsymbol{\omega}$, is considered. The total torque in this situation can be expressed in terms of the normal velocity of each asperity, v_n^i, the dissipative coefficient in the contact law, η_n, and the tangential distance from each contact point to the centre of mass, $\boldsymbol{d}_t$. As the system is symmetrical, the asperities move with equal and opposite velocities, $\boldsymbol{v}_n^1 = -\boldsymbol{v}_n^2 = \boldsymbol{v}_n$ The torque can then be expressed as

$$\begin{aligned}\boldsymbol{\tau}_{\text{sym}} &= -2\eta_n \boldsymbol{d}_t \times v_n \\ &= -2\eta_n \boldsymbol{\omega}|\boldsymbol{d}_t|^2.\end{aligned} \tag{49}$$

For the sake of simplicity, the value of the average torque applied as each asperity comes in and out of contact is assumed to be some fraction of this total. $\bar{\boldsymbol{\tau}}_{\text{asp}} = \xi\boldsymbol{\tau}_{\text{sym}}$. The constant ξ is expected to be small, as the torque given by Eq. (49) is only realised for a relatively small amount of time. For most of the time as a particle rolls there is not a significant velocity at the contact point.

The value of $\boldsymbol{\tau}_{\text{asp}}$ depends on the contact model used, and this derivation relies on the contact model describing visco-elastic forces in the contact. In the present study the damping term, η_n, given by Eq. (16), depends on a number of properties of the particle material and the collision. These are the parameter η_n, which characterises the incomplete restitution of velocity during a normal impact, the particle mass, M, the radius at the point of contact, r_{asp}, the reduced elastic modulus, E^*, and the current overlap at the contact point, δ_n. However, the steps outlined presently could be adapted to any other contact model which uses a dissipative term proportional to the normal velocity at the collision.

In a 3D system the value of $n_{2\pi}$ must also be approximated. Depending on the orientation of the particle as it rolls, it is possible that a greater or smaller number of asperities may come into contact. If the density of asperities on the surface, D_p, and average radius, R_0, are known, and the asperities are evenly distributed over the surface, then the number of expected contacts over the course of one complete revolution can be approximated as

$$n_{2\pi} = R_0\sqrt{\frac{2}{\sqrt{3}D_p}}. \tag{50}$$

Eqs. (48) to 50 give a method of calculating the torque experienced by a rolling particle. Due to the dependency of $\boldsymbol{\tau}_{\text{sym}}$ on $\boldsymbol{\omega}$, the decelerating torque takes the form

$$\begin{aligned}&\bar{\boldsymbol{\tau}}_{\text{decel}} = -\gamma\boldsymbol{\omega}, \text{ where} \\ &\gamma = -2\xi\eta_n|\boldsymbol{d}_t|^2 n_{2\pi}.\end{aligned} \tag{51}$$

A torque of this form leads to the exponential decay of angular velocity. The parameter ξ remains to be determined, and may need to be fit to data. Whereas in the case of the torque experienced by stationary particles under a tangential force the parameters λ_F and λ_ϕ are bounded to a small region, ξ may take a wide range of values. It is certain that $\xi < 1$, and likely that $\xi \ll 1$, however due to the approximate nature of the model it is difficult to constrain its value further.

5. Results

The models presented in Section 4 give predictions for the force and angle of initial rolling, as well as the rate at which rolling particles slow down. However, the parameters $\lambda_{\boldsymbol{\tau}}$ from Eq. (45), λ_ϕ, from Eq. (47), and ξ, from Eq. (51), remain to be determined. In order to test the validity of the models, and ascertain values for these parameters, simulations of rolling particles have been performed.

Numerical results are produced for particles with an average radius of 40 μm. Roughnesses are simulated with various values for the standard deviation of surface height, σ_r, and the correlation length, l_c. σ_r is varied in the range 0.5μm to 1.6μm, and l_c from 4.5μm to 6.5μm. Particles with roughnesses of these bounding values can be seen in Fig. 1. These roughnesses are chosen as they represent a

range of surfaces, from a particle which is almost smooth to one with many high peaks.

The properties of simulated particles are summarised in Table 1. A relatively high coefficient of friction of $\mu = 0.4$ is chosen so that the contacts do not slip upon the application of a tangential force. This is important as a sliding particle is less inclined to roll, and it is more difficult to assess the rolling behaviour in a particle which exhibits significant sliding motion.

5.1. Rolling resistance of a stationary particle

5.1.1. Simulation setup

The rolling of rough particles is studied using DEM simulations. To set up a simulation, it is first necessary to generate a particle with the required values of σ_r and l_c, using the method described in Section 3.4. As the generation initially involves the random placement of asperities, each particle generated is geometrically different but statistically equivalent. The particle is then inserted into a DEM simulation domain with solid walls, and allowed to settle on the lower wall under the influence of gravity. Enough time is allowed to elapse that the particle's velocity and rotational velocity are negligibly small.

To study the initial rolling of a stationary particle, a tangential force is applied in one direction. The magnitude of this force starts at zero and linearly increases, at a slow enough rate that the system can be considered to be in static equilibrium at all times. At the critical force, the particle contacts exert the maximum torque they are capable of in response to a tangential force in that direction. As the force surpasses this value the particle starts to roll, at which point the simulation is stopped. At every timestep the torque exerted by the particle contacts and the angle of rotation of the particle are output, so that the critical torque and angle may be determined. The angle rolled as a function of tangential force in this type of simulation is shown in Fig. 5. As the force increases, the angle increases linearly until close to the critical angle, $\bar{\phi}^{\text{crit}}$. Near to this point the behaviour transitions, as the particle transitions from a static to a dynamic state, and the angle increases rapidly.

5.1.2. Numerical results

The maximum tangential force a stationary particle can withstand, and the angle at which it starts to roll, are determined by numerical simulation. This allows a comparison to be made between these values and the analytical predictions. The critical torque and angle at which a particle starts to roll are given by Eqs. (45) and (47) respectively. These values have been determined for the range of values of σ_r and l_c specified in Section 5.

Comparisons between the critical torque found via simulations and analytically for particles with and without adhesion are presented in Figs. 6 and 7 respectively. Each point in these plots is the result of averaging over 30 simulations. This averaging is necessary to account for variations due to the orientation of the particle with respect to the direction in which the force is applied. The parameter in the model which takes this averaging into account, λ_τ, introduced in Eq. (45), is found to have a value of $\lambda_\tau = 0.45$. This parameter was determined to be constrained to the range $0.5 \leq \lambda_\tau \leq 1$, however actually falls just outside this range. It is thought that this is due to the assumption in Section 4.1.1 that the contact points form an equilateral triangle. Small deviations from this idealised geometry are likely to lead to lower values for the critical torque, lowering the average value.

Table 1
A summary of particle properties. The work of adhesion only applies to the simulations of adhesive particles, for non-adhesive systems it takes a value of 0 J m^2.

Particle properties	
Average radius, R_0	40μm
Density, ρ	1250 kg m^{-3}
Elastic modulus, E	1×10^7 Pa
Poisson ratio, ν	0.33
Coeff. friction, μ	0.4
Coeff. restitution, e	0.8
Work of adhesion, $\Delta\gamma$	5×10^{-5} J m^{-2}

Fig. 6 shows that in non-adhesive case the force required to initiate rolling increases with increasing σ_r for all values of l_c. To explain this, we note that the distance parallel to the bottom wall from the centre of mass to each contact, d_t, increases with σ_r. The torque which can be applied by the contacts in each case is therefore larger, for the same contact force. When there are adhesive interactions, this is not necessarily the case. For small values of l_c the critical force is predicted to be larger for smaller values of σ_r. This can be explained by the dependence of the adhesive forces on the asperity radius. Smaller values of l_c will lead to larger asperity radii, and therefore greater adhesive forces. It can be seen in Fig. 7 that the increase in adhesive forces compensate for the decrease in d_t for low values of l_c.

For both adhesive and non-adhesive particles, an increase in l_c increases the range of forces observed as σ_r changes. It might be thought that increasing the correlation length would also increase d_t, as the distance between asperities does increase. However, the corresponding increase in asperity radius means that when a particle rests on a plane, the distance d_t is actually smaller.

From the same simulations, the critical angle at which rolling begins is determined. Numerical results, compared to the analytical model of the critical angle are shown in Fig. 8 for the non-adhesive case, and Fig. 9 for the adhesive case. The analytical expression, Eq. (47), is found to fit best when the parameter λ_ϕ takes a value of $\lambda_\phi = 0.85$.

The angles at which particles start to roll tend to follow the opposite trend to the forces: particles which require a higher force often roll at a smaller angle. This is also a product of the effects of asperity radius. Asperities with smaller radii do not need to deform as much to provide the same force, and therefore the value of δ in Eq. (36) is smaller. In this case adhesive interactions amplify the effect. Asperities with stronger adhesive interactions – those with a larger radius – will have larger values of δ due to the increased normal force.

The agreement between the analytic model and the simulated systems is not exact; however it is sufficiently close that a system of particles simulated using the analytic model should display bulk behaviour similar to that of the rough particles being simulated.

5.2. Slowing of rolling particles

5.2.1. Simulation setup

When investigating the slowing of rolling particles, a particle is generated and allowed to settle in the manner described in

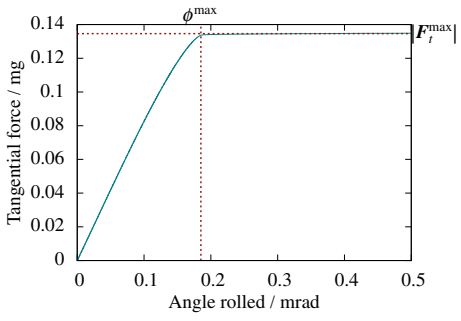


Fig. 5. A typical example of the angle rolled by a rough particle as a tangential force which slowly, linearly increases with time is applied. This case corresponds to a non-adhesive particle with an average radius of 40×10^{-6} m, with roughness parameters $\sigma_r = 1\times10^{-6}$ m and $l_c = 5\times10^{-6}$ m.

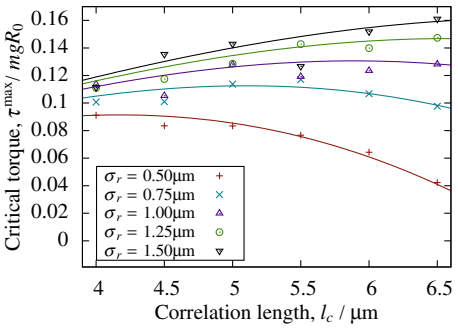


Fig. 6. Dimensionless critical torque at which rolling occurs for non-adhesive particles. Each point represents the average value of 30 simulations, with sets of points corresponding to different values of the standard deviation of surface height, σ_r. Lines are the results of the analytic model, coloured to match the corresponding numerical data.

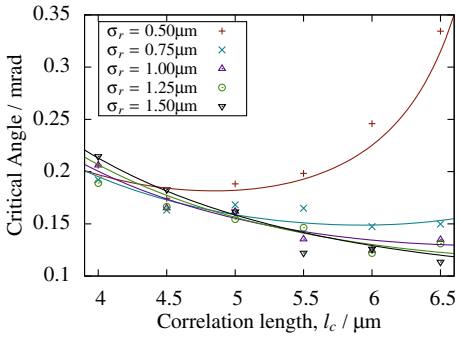


Fig. 8. Critical angle at which rolling occurs for non-adhesive particles. Each point represents the average value of 30 simulations, with sets of points corresponding to different values of the standard deviation of surface height, σ_r. Lines are the results of the analytic model, coloured to match the corresponding numerical data.

Section 5.1.1. A constant, relatively high, tangential force is then applied. This instigates a rolling motion in the particle. After 0.025 s the force is removed, and the particle allowed to decelerate. The linear and angular velocities are output every timestep so that the deceleration may be analysed.

Fig. 10 shows the velocity of a particle in this type of simulation as a function of time. Typical behaviour in this type of simulation is a linear acceleration while the force is applied, followed by a deceleration until the particle is stationary. The deceleration is typically initially linear, but transitions to a non-linear deceleration, which is modelled well by an exponential decay of velocity. During the linear deceleration at higher velocities, the particle is observed to be bouncing, and spends most of its time out of contact with the bottom wall. Then, when the particle stops bouncing, it enters the second regime of rolling while in constant contact with the wall. This second regime corresponds to that described in Section 4.2.

5.2.2. Numerical results

Simulations of rolling particles have been performed using the method described in Section 5.2.1. In this case for each combination of σ_r and l_c the simulation is repeated 25 times, and the results averaged. By fitting a continuous function consisting of a linear component followed by an exponential decay to each of the velocity profiles, the value of the decay constant is ascertained. An example of this fit is shown in Fig. 10. The linear region of deceleration, while necessary to accurately fit the data, is not described by the analytical model. Rolling resistance typically has greatest influence in systems of low kinetic energy – in a sand pile, for instance, it is the onset of rolling which is important rather than the high velocity behaviour. It is not, therefore, considered critical to model the higher velocity behaviour in detail.

The rolling coefficient γ, as defined in Eq. (51), has been determined via simulations for the range σ_r and l_c used in Section 5.1. The observed values for γ are shown in Figs. 11 and 12, along with the values given by Eq. (51). Eqs. (48) to (50) are found to agree well with the results from simulated particles for a value of $\xi = 5 \times 10^{-4}$. For both adhesive and non-adhesive cases the value of γ is observed to increase with increasing values of σ_r. This is largely due to the increase in $|d_t|$ as σ_r increases, which leads to larger torques applied by the contacts. The dependence of γ on l_c is more complex, with several competing factors.

The difference in γ values between the non-adhesive and adhesive particles is relatively small. Adhesive particles slow down slightly faster in all cases, but does not appear to strongly interact with the roughness properties. This is due to the weak dependence of Eq. (16) on the normal force: $\eta_n \sim |\boldsymbol{F}_n|^{1/6}$.

5.3. DEM implementation

Rolling resistance due to roughness and adhesion can be modelled in DEM using the theoretical approach described in Section 4. The standard deviation of surface height and correlation length, σ_r and l_c, and the work of adhesion, $\Delta\gamma$, must be input as additional particle properties.

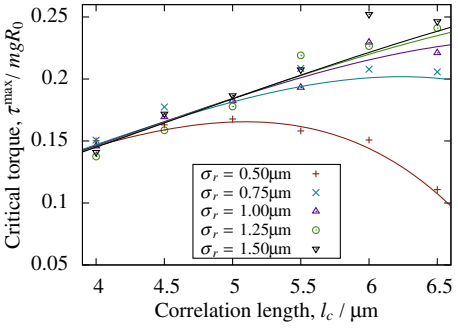


Fig. 7. Dimensionless critical torque at which rolling occurs for adhesive particles. Each point represents the average value of 30 simulations, with sets of points corresponding to different values of the standard deviation of surface height, σ_r. Lines are the results of the analytic model, coloured to match the corresponding numerical data.

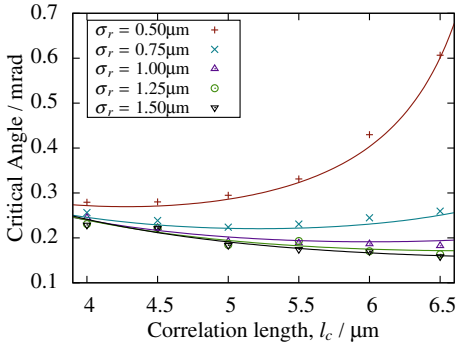


Fig. 9. Critical angle at which rolling occurs for adhesive particles. Each point represents the average value of 30 simulations, with sets of points corresponding to different values of the standard deviation of surface height, σ_r. Lines are the results of the analytic model, coloured to match the corresponding numerical data.

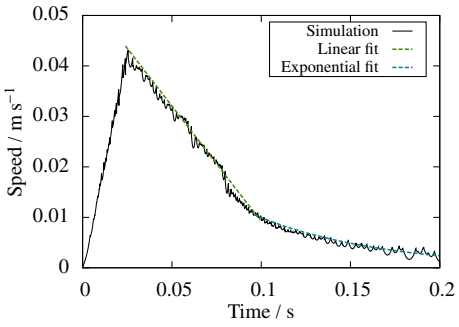


Fig. 10. The speed of a particle as it is accelerated and allowed to decelerate. In this case the particle has σ_r =1 μm, l_c = 5μm. A constant tangential force is applied until $t = 0.025$. When the particle is allowed to decelerate, it initially does so in a linear fashion – in this regime the particle is bouncing, with asperities making occasional contact with the ground. Once the particle slows sufficiently that it is no longer bouncing, it loses speed in an exponential fashion. Dashed lines correspond to the linear and exponential functions fitted to the data to characterise the deceleration.

The torques which arise due to the asymmetrical distribution of normal forces in the static case, described in Section 4.1, average to zero as the particle rolls. It is therefore necessary to define the transition from the static to the dynamic case as the particle starts rolling. While the model was derived under the assumption of static equilibrium, in a real system it is rarely the case that the angular velocity $\boldsymbol{\omega} = 0$. The initial rolling resistance is only applied when the total kinetic energy of the particle must be sufficiently small that it cannot roll over one asperity under its own momentum. With the average asperity height given by Eq. (9),

$$\frac{1}{2}mv^2 + \frac{1}{2}I\boldsymbol{\omega}^2 < F_n\frac{4\sigma_r}{\sqrt{3\pi}}. \tag{52}$$

At low velocities, the torque applied by the dynamic rolling model is small, and including the term proportional to $\boldsymbol{\omega}$ helps to stabilise the system and avoid oscillations. In this regime, the rolling resistance torque on a DEM particle is therefore a sum of the static and dynamic cases:

$$\boldsymbol{\tau}_r = \boldsymbol{\tau}_s + \boldsymbol{\tau}_d, \tag{53}$$

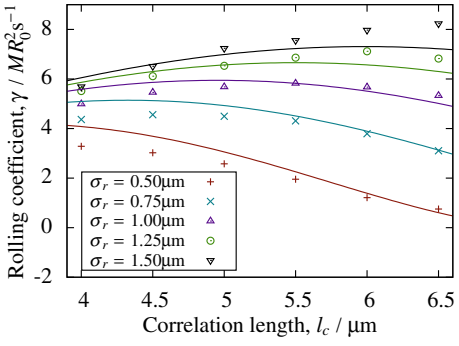


Fig. 11. Rolling drag coefficients for non-adhesive particles. Each point represents the average value of 25 simulations, with sets of points corresponding to different values of the standard deviation of surface height, σ_r. Lines are the results of the analytic model, coloured to match the corresponding numerical data.

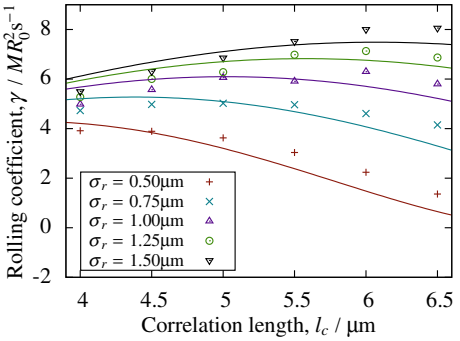


Fig. 12. Rolling drag coefficients for non-adhesive particles. Each point represents the average value of 25 simulations, with sets of points corresponding to different values of the standard deviation of surface height, σ_r. Lines are the results of the analytic model, coloured to match the corresponding numerical data.

where

$$\boldsymbol{\tau}_s = \begin{cases} -\bar{\boldsymbol{\tau}}^{\text{crit}}\frac{\phi_r}{\bar{\phi}^{\text{crit}}}\frac{\boldsymbol{\omega}}{|\boldsymbol{\omega}|}, & \text{if } |\boldsymbol{\tau}_r| < \bar{\boldsymbol{\tau}}^{\text{crit}} \\ -\bar{\boldsymbol{\tau}}^{\text{crit}}\frac{\boldsymbol{\omega}}{|\boldsymbol{\omega}|}, & \text{otherwise} \end{cases} \tag{54}$$

$$\boldsymbol{\tau}_d = -\gamma\boldsymbol{\omega}. \tag{55}$$

At higher velocities it is only necessary to consider the dynamic rolling resistance, $\boldsymbol{\tau}_d$.

In these equations, $\bar{\boldsymbol{\tau}}^{\text{crit}}$ and $\bar{\phi}^{\text{crit}}$ are given by Eqs. (45) and (47) respectively, with coefficients $\lambda_{\boldsymbol{\tau}} = 0.45$ and $\lambda_\phi = 0.85$. Similarly, γ is given by Eq. (51), with the coefficient $\xi = 5 \times 10^{-4}$.

6. Discussion and conclusions

In this paper, a model has been developed to describe the resistance to rolling of rough particles, which may be adhesive. The causes and effects of rolling resistance have been investigated previously, and models developed to describe the rolling of spheres with various interactions taken into account. However, the significant role played by the interplay of surface roughness and adhesive contacts has not been previously considered. The insight gained in this study is valuable in providing a physical motivation for the observed immobility of fine powders, and a model of this phenomena which is suitable for DEM simulations. It can be seen that not only are adhesive forces relatively stronger in smaller powders, but that they also play a part in restricting rolling motion.

In the analytical model rough surfaces are parametrised using the average properties of correlated random fields. This helps to constrain the potentially enormous parameter space to only surface profiles which could reflect real roughnesses. The model consists of expressions for the critical angle and torque at which a rough particle starts to roll, as well as the rate at which they decelerate. Each part of the model contains one unknown parameter, which requires fitting to results obtained by simulating the equivalent particles using DEM. The fitted curves are in good agreement with the average behaviour of the DEM simulations of rough particles. The result of this is that instead of performing expensive simulations of compound particles, it is possible to simulate spheres which behave in a very similar manner. The most detailed roughness simulated in the present study consisted of a central sphere, with 115 asperities. To simulate a system of these compound particles would be on the order of 100 times slower than a simulation in which each particle is represented by a

single sphere, using the new rolling resistance model. Such developments increase the size of systems which may be simulated, while maintaining accurate particle interactions.

In comparison to previous models of rolling resistance, the new model is similar in some ways to existing approaches. The torque experienced by static particles takes a form similar to that of Iwashita and Oda [48]. A significant difference is that in this case the torque is only applied during onset of rolling, whereas in the original formulation the torque stays at the critical value that it reaches. Rolling particles slow at a rate proportional to their velocity. The expression is similar to the model proposed by Zhou et al. [10], albeit with a more complex dependency on the collision and particle properties.

Due to the stochastic nature of surface roughness, it is impossible to accurately reproduce all behaviour in a model simple enough to be used in DEM. While average rolling resistance is accurately replicated, the contact between a real rough particle and the plane will not necessarily follow this average due to the details of the geometry. However, in a system of many particles it is often the case that the average behaviour dominates. While variations around the average may have a large effect on the motion of each individual particle, the statistical behaviour of a system of many particles will not be significantly changed.

The model has been derived for contact between a rough particle and a plane. The contact forces in contacts between two particles will be different, and effects such as interactions between asperities make the system far more complex, however the general principle upon which the model is based still applies. Furthermore, the model is only applicable in the regime where asperities will not come into contact as a result of elastic deformation. For particles in which the correlation length of the largest scale of roughness is very short compared to the particle radius, more than three asperities will come into contact as the particle deforms. For such cases the model presented is not applicable. When roughness occurs on multiple scales, it may be the case that what appear to be contact areas may in fact consist of many contacts, due to roughness on a smaller scale. In this instance the model may in some cases provide an adequate approximation of rolling resistance, but only when torques are dominated by the largest scale of roughness.

In summary, a model of the rolling resistance due to particle non-sphericity and adhesion has been developed. This model can be used in the study of dry, rough powders, which may exhibit adhesive interactions. The additional resistance to rolling due to adhesive forces may help to shed light on the mechanism governing phenomena such as avalanches and collapses.

Acknowledgments

Robert Wilson was supported through a studentship in the Centre for Doctoral Training on Theory and Simulation of Materials at Imperial College London funded by the Engineering and Physical Sciences Research Council under grant number EP/G036888/1.

Daniele Dini also acknowledges the support of the Engineering and Physical Sciences Research Council under his Established Career Fellowship, grant number EP/N025954/1. Data reported in this paper can be obtained upon request by emailing tribology@imperial.ac.uk.

References

[1] H. Teufelsbauer, Y. Wang, S.P. Pudasaini, R.I. Borja, W. Wu, DEM simulation of impact force exerted by granular flow on rigid structures, Acta Geotech. 6 (3) (2011) 119–133.
[2] D. Geldart, Gas Fluidization Technology, John Wiley & Sons, Bradford, 1986.
[3] Z.B. Tong, B. Zheng, R.Y. Yang, A.B. Yu, H.K. Chan, CFD-DEM investigation of the dispersion mechanisms in commercial dry powder inhalers, Powder Technol. 240 (2013) 19–24.
[4] J.a. Greenwood, J.H. Tripp, The elastic contact of rough spheres, J. Appl. Mech. 34 (1967) 153.
[5] J.A. Greenwood, J.J. Wu, Surface roughness and contact: an apology, Meccanica 36 (6) (2001) 617–630.
[6] J. Visser, Van der Waals and other cohesive forces affecting powder fluidization, Powder Technol. 58 (1) (1989) 1–10.
[7] J.A. Mousel, J.S. Marshall, Aggregate growth and breakup in particulate suspension flow through a micro-nozzle, Microfluid. Nanofluid. 8 (2) (2010) 171–186.
[8] P.A. Cundall, O.D.L. Strack, A discrete numerical model for granular assemblies, Géotechnique 29 (1) (1979) 47–65.
[9] J.S. Curtis, B.G.M. van Wachem, Modeling particle-laden flows: a research outlook, AICHE J. 50 (11) (2004) 2638–2645.
[10] Y. Zhou, B. Wright, R. Yang, B. Xu, A. Yu, Rolling friction in the dynamic simulation of sandpile formation, Phys. A 269 (1999) 536–553.
[11] V. Frette, K. Christensen, A. Malthe-Sørenssen, J. Feder, T. Jøssang, P. Meakin, Avalanche dynamics in a pile of rice, Nature 379 (6560) (1996) 49–52.
[12] N. Brilliantov, T. Pöschel, Rolling friction of a viscous sphere on a hard plane, Europhys. Lett. 42 (5) (1998) 511–516.
[13] T. Poeschel, T. Schwager, N.V. Brilliantov, Rolling friction of a hard cylinder on a viscous plane, Eur. Phys. J. B 10 (1) (1998) 7.
[14] Q.J. Zheng, H.P. Zhu, A.B. Yu, Finite element analysis of the rolling friction of a viscous particle on a rigid plane, Powder Technol. 207 (1-3) (2011) 401–406.
[15] N. Brilliantov, T. Pöschel, Rolling as a continuing collision, Eur. Phys. J. B 12 (2) (1999) 299–301.
[16] K.R. Eldredge, D. Tabor, The mechanism of rolling friction. I. The plastic range, Proc. Royal Soc. A Math. Phys. Eng. Sci. 229 (1955) 181–198.
[17] K. Johnson, K. Kendall, A. Roberts, Surface energy and the contact of elastic solids, Proc. Royal Soc. London. A. Math. Phys. Sci. 324 (1558) (1971) 301.
[18] C. Dominik, a.G.G.M. Tielens, Resistance to rolling in the adhesive contact of two elastic spheres, Philos. Mag. A 72 (3) (2006) 783–803.
[19] S. Krijt, C. Dominik, A.G.G.M. Tielens, Rolling friction of adhesive microspheres, J. Phys. D. Appl. Phys. 47 (1) (2014) 175302.
[20] C.M. Wensrich, A. Katterfeld, Rolling friction as a technique for modelling particle shape in {DEM}, Powder Technol. 217 (2012) 409–417.
[21] F. Beer, E.R.J.r. Johnston, J. DeWolf, D. Mazurek, Mechanics of Materials, McGraw-Hill Education. 2011.
[22] Y.C. Zhou, B.H. Xu, a.B. Yu, P. Zulli, Numerical investigation of the angle of repose of monosized spheres., Phys. Rev. E 64 (2) (2001) 021301.
[23] R.D. Mindlin, H. Deresiewicz, Elastic spheres in contact under varying oblique forces, J. of Appl. Mech. 20 (1953) 327–344.
[24] J. Ai, J.-F. Chen, J.M. Rotter, J.Y. Ooi, Assessment of rolling resistance models in discrete element simulations, Powder Technol. 206 (3) (2011) 269–282.
[25] A.W. Bush, R.D. Gibson, T.R. Thomas, The elastic contact of a rough surface, Wear 35 (1) (1975) 87–111.
[26] P.R. Nayak, Random process model of rough surfaces, J. Lubr. Technol. 93 (1971) 398–407.
[27] D.J. Whitehouse, J.F. Archard, The properties of random surfaces of significance in their contact, Proc. Royal Soc. London. A. Math. Phys. Eng. Sci. 316 (1524) (1970) 97–121.
[28] J.a. Greenwood, J.B.P. Williamson, Contact of nominally flat surfaces, Proc. Royal Soc. A. Math. Phys. Eng. Sci. 295 (1966) 300–319.
[29] J.I. McCool, Comparison of models for the contact of rough surfaces, Wear 107 (1) (1986) 37–60.
[30] Y. Tsuji, T. Tanaka, T. Ishida, Lagrangian numerical simulation of plug flow of cohesionless particles in a horizontal pipe, Powder Technol. 71 (3) (1992) 239–250.
[31] K. Johnson, Contact Mechanics, Cambridge University Press, Cambridge, UK, 2003.
[32] S.B. Kuang, K.W. Chu, A.B. Yu, Z.S. Zou, Y.Q. Feng, Computational investigation of horizontal slug flow in pneumatic conveying, Ind. Eng. Chem. Res. 47 (2) (2008) 470–480.
[33] N.V. Brilliantov, F. Spahn, J.-M. Hertzsch, T. Pöschel, Model for collisions in granular gases, Phys. Rev. E 53 (5) (1996) 5382–5392.
[34] N.V. Brilliantov, A.V. Pimenova, D.S. Goldobin, A dissipative force between colliding viscoelastic bodies: rigorous approach, Europhys. Lett. 109 (1) (2015) 14005.
[35] Q.J. Zheng, H.P. Zhu, A.B. Yu, Finite element analysis of the contact forces between a viscoelastic sphere and rigid plane, Powder Technol. 226 (2012) 130–142.
[36] B. Derjaguin, Effect of contact deformations on the adhesion of particles, J. Colloid Interface Sci. 53 (2) (1975) 314–326.
[37] V. Muller, B. Derjaguin, Y. Toporov, On two methods of calculation of the force of sticking of an elastic sphere to a rigid plane, Colloids Surf. 7 (1983) 251–259.
[38] H. Hamaker, The London van der Waals attraction between spherical particles, Physica 4 (1937) 1058–1072.
[39] D. Tabor, Surface forces and surface interactions, J. Colloid Interface Sci. 58 (1) (1977) 2–13.
[40] J.A. Greenwood, On the DMT theory, Tribology Letters 26 (3) (2007) 203–211. ISSN 10238883.
[41] D. Maugis, Adhesion of spheres: the JKR-DMT transition using a Dugdale model, J. Colloid Interface Sci. 150 (1) (1992) 243–269.
[42] S. Ecke, H.-J. Butt, Friction between individual microcontacts, J. Colloid Interface Sci. 244 (2001) 432–435.
[43] J.a. Greenwood, Adhesion of elastic spheres, Proc. Royal Soc. A. Math. Phys. Eng. Sci. 453 (1961) (1997) 1277–1297.
[44] B. van Wachem, M. Zastawny, F. Zhao, G. Mallouppas, Modelling of gas–solid turbulent channel flow with non-spherical particles with large Stokes numbers, Int. J. Multiphase Flow 68 (2015) 80–92.

[45] F. Zhao, B. van Wachem, Direct numerical simulation of ellipsoidal particles in turbulent channel flow, Acta Mech. 224 (10) (2013) 2331–2358.
[46] F. Zhao, B. van Wachem, A novel Quaternion integration approach for describing the behaviour of non-spherical particles, Acta Mech. 224 (12) (2013) 3091–3109.
[47] G. Marsaglia, Choosing a point from the surface of a sphere, Ann. Math. Stat. 43 (2) (1972) 645–646.
[48] K. Iwashita, M. Oda, Rolling resistance at contacts in simulation of shear band development by DEM, J. Eng. Mech. 285 (1998) 285–292.